3D Printed Physics: Using Modular Components for Optimized High-Field Electron Paramagnetic Resonance Sample Manipulation

Leonardo Ramirez-Mireles
Department of Physics, University of California, Santa Barbara
Department of Physics, Rice University

Faculty Advisor: Prof. Mark Sherwin
Post Doctoral Advisor: Dr. Antonín Sojka
Department of Physics, University of California, Santa Barbara
Institute for Terahertz Science and Technology

(Dated: October 1, 2024)

ABSTRACT

Electron paramagnetic resonance (EPR) spectroscopy is a powerful technique used to study samples with free electrons in a broad range of industries, including medical and scientific fields. High-field EPR (HF-EPR) spectrometers, which operate in the sub-THz range, are extremely sensitive and have a temporal resolution on the order of nano-seconds, enabling studies of zero field splitting phenomena at high resolutions. Typically, EPR data is collected using a probe (a waveguide with a dedicated sample holder assembly at the bottom) centered in a high magnetic field. Beyond this, instrumentation for high-field applications is often lab-built with varying parameters and low sample throughput that present challenges to a consistent quantitative workflow. The implementation of simple feedthroughs allows for smart mechanical design to expand the capabilities of EPR probes operating in low vacuum and at cryogenic temperatures. The solution presented here outlines the design and manufacturing of a modular, 3D-printable system that can cycle through samples and withstand temperatures between 2-300K in magnetic fields as high as 16 T. Via a dedicated airlock the inside of the probe is easily accessed, enabling high sample throughput that reduces the time needed to collect data in 170-500 GHz EPR experiments by as much as 50 hours per cycle. As a proof of concept, a simplified sample holder was printed and tested for field homogeneity, showing the potential for novel 3D printed instrumentation in experimental physics.

I. INTRODUCTION

Electron paramagnetic resonance (EPR) spectroscopy is versatile technique used to study samples with free electrons in a broad range of industries, including medical and scientific fields. High-field EPR (HF-EPR) spectrometers operating in the sub-THz range are particularly useful; Samples are irradiated with microwave radiation, essentially non-invasive, and spectral and temporal resolutions are high enough that scientists are able to study detailed zero-field splitting phenomena. High-field spectrometers can also enable the characterization of samples on the nano-scale [1], which drastically decreases the amount of sample needed for a useful spectra. In some cases, spin tags are able to extend these capabilities to protein studies, providing biologists and biophysicists with a powerful lens for microscopic movements [2]. Since the incident radiation is microwave-based, EPR experiments are nominally invasive, allowing for the detailed study of living organisms [3]. In some cases, EPR has even been used in medical fields to quantify radiation doses administered in cancer treatments [4].

The underlying principle behind EPR (and similarly, NMR) spectroscopy is known as the Zeeman effect. All electrons have a spin of either ± 1/2, which in turn gives them an intrinsic magnetic moment given by the following expression:

$$\mu_s = -g_e \mu_b \frac{S}{\hbar}. \tag{1}$$

Where μ_b is the bohr magneton constant $(9.274x10^{-24} J/T)$, g_e is the unitless g-factor constant($\approx$ 2), and S is the electron spin angular momentum. In EPR applications, electrons are placed in a magnetic field, causing their dipoles to accrue some amount of potential energy taking the form,

$$U = -\mu_s \cdot B. \tag{2}$$

If we consider that the magnetic dipoles eventually align either parallel or antiparallel to B, which is experimentally set to be in the z-direction, then $S_z = m_s \hbar$. Here, m_s is the spin quantum number, $\pm\frac{1}{2}$ for electrons. The potential energy becomes,

$$U = -g_e \mu_b m_s B = \pm\frac{1}{2} g_e \mu_b B. \tag{3}$$

We see then that the potential energy is proportional only to the external magnetic field. (4) models the theoretical energy difference ΔE:

$$\Delta E = g_e \mu_b B = h\nu. \tag{4}$$

In the absence of an external magnetic field, these two magnetic moments have the same energy. As B increases, this degeneracy is lifted, leading to Zeeman splitting of spectral lines. The Boltzmann distribution models that more electrons assume the lower energy (spin up) state, meaning transitions register as a net absorption, as shown in Fig. 1.

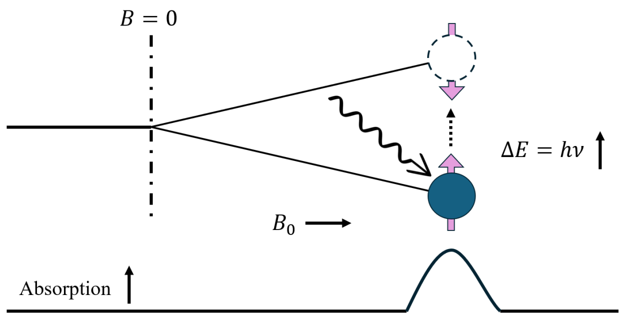

FIG. 1. Zeeman splitting is directly proportional to B_0. From quantum mechanics, we know we can "excite" lower energy electrons with incident electromagnetic radiation at a specific wavelength ν. This excitation is registered as an absorption, yielding information about the surrounding paramagnetic environment.

II. BACKGROUND

High-field EPR spectrometers, like the one used at UCSB's Institute for Terahertz Science and Technology (ITST) operate under more extreme conditions than commercially available instrumentation, but present the possibility for more detailed spectra. In order to achieve such high resolution, there are a few key components commonly found in most EPR setups. There is a large (in our case up to $\pm 12.5T$) superconducting electromagnet, which (with a series of smaller magnets) is able to precisely sweep through fields and collect data in the form of the first derivative of absorption, as shown in Fig. 2.

Centered in this magnetic field lies the probe, as shown in Fig. 6, which crucially features a corrugated waveguide matching the (240 GHz) microwave frequency. At the bottom of the waveguide, in the strongest part of the magnet lies the sample holder which houses the sample of interest, focuses the microwave beam and reflects it back towards the microwave bridge where it is then collected and further analyzed. Depending on the sample and holder, measurements can be taken at variable temperatures from 300K (room temp) to 2K (liquid helium). Sample holders also include a modulation coil, which finely sweeps through a small region of B, contributing to the signal formation.

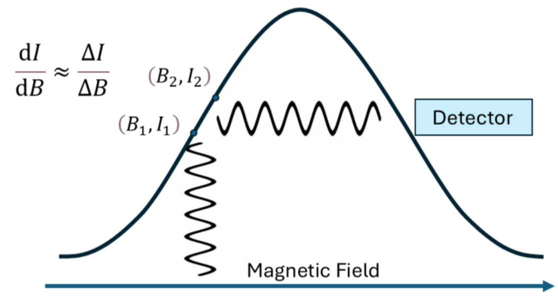

FIG. 2. EPR data is collected by measuring changes in intensity of absorbed light I while sweeping the magnetic field B using the larger superconducting magnets and the modulation coil. As sweeping steps get smaller, the plotted data approaches the first derivative of absorption.

Often, a vacuum is necessary to avoid microwave losses. Moisture in the air can condense into water, and then ice at the low temperatures, making it a great microwave absorber. Oxygen also poses an issue. Since its structure features a diradical, it can also experience Zeeman splitting, producing a pronounced signal. In medical applications, this effect has been exploited to measure tissue oxygenation [4], but typically it's treated as noise in condensed matter settings.

Within the context of high-field EPR, 240 GHz is relatively high-two orders of magnitude above the norm. This is in part motivated by the study of zero-field splitting phenomenon, secondary splitting patterns that occur in systems where spin, S $> \frac{1}{2}$. Additionally, the high frequencies greatly increase spectral resolution, having profound benefits for biochemistry and biophysics applications. This is because the lowest number of detectable spins, N, generally varies inversely to the frequency used [5], making ultra-high frequencies useful for resolving very low N systems.

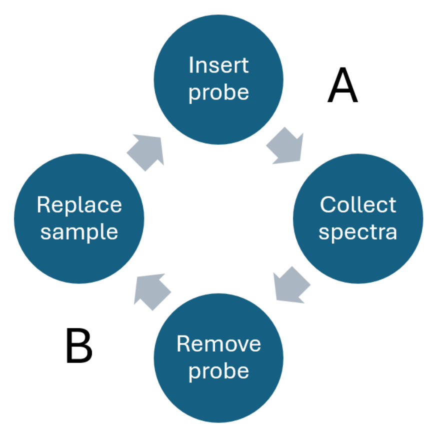

FIG. 3. Here's the current workflow for collecting a spectra using a HF-EPR spectrometer. A: Wait for probe to cool down, create vacuum B: Let probe temperature re-equilibrate, and release vacuum. Total time per sample : approx. 8 hours

Currently, the ITST is building a new high-field EPR setup with the intent of installing a more powerful, 16 T magnet. The setup is designed to be tuneable to multiple frequencies (as high as 500 GHz), enabling a broader range of experiments. Furthermore, there are plans for a dedicated sample cooling system to bring samples down to sub-liquid helium temperatures (300K-2K). This would greatly increase the spectrometer's capabilities but requires the probe to reach a thermal equilibrium before collecting a sample's spectra; a process that takes 8 or more hours depending on sample type.

Most sample holders typically house a single sample at a time, partly because of the harsh pressure and temperature conditions, but also because of size restrictions imposed by the magnet's inner profile. Moreover, there is an absence of research into the types of materials and mechanisms that operate reliably through such extreme pressure and temperature cycles. Because of this, the current workflow, shown in Fig. 3, is slow and at times repetitive. There has been an effort to increase the sample capacity of typical sample holders [6], but it's difficult to have instrumentation that can be readily manufactured and customized in the lab. As such, we turn towards achieving a more streamlined process using a modular system, with parts designed using web-based CAD software and manufactured using commercially available 3D printers.

III. CURRENT 3D MODELS AND DESIGN GOALS

The figures presented here are derived from existing models created by Dr. Antonín Sojka and Brad Price for the new high-field setup under construction at the ITST.

The quasi-optical sample holder shown in Figure 4, features a variation of the roof mirror assembly that successfully increased the SNR in a previously published design [7]. The optimized mirror assembly leaves room for a piezo-electric motor, allowing precise control of sample location. As it is, this design only has room for a single sample.

Figure 5 is a rendering of the new probe for the 16 T setup. This new probe features an airlock, which gives users the ability to access a reduced space inside of the probe. The profile along the length of the waveguide is simple with periodic copper heat shields, ensuring low temperatures inside the magnet. There is also a mechanical feedthrough, which gives some degree of motion inside of the probe. It was thought that this could be used as a way to manipulate samples, but there were no previous outstanding solutions.

As such, the goal of this project was to fully design a system to hold multiple samples and use the feedthrough to safely cycle through them, enabling quantitative measurements and lower downtime between experiments. Because high-field experiments require rather extreme conditions, there are a few design constraints that the

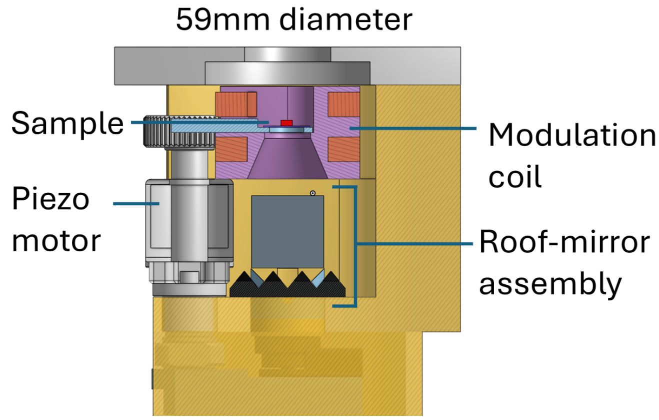

FIG. 4. Here's a cross-section of the new QOSH. The top connecting flange (silver) has a 59mm diameter, designed to fit inside the magnet's 60mm bore. The modulation coil (orange) is used to sweep B around the sample at the center.

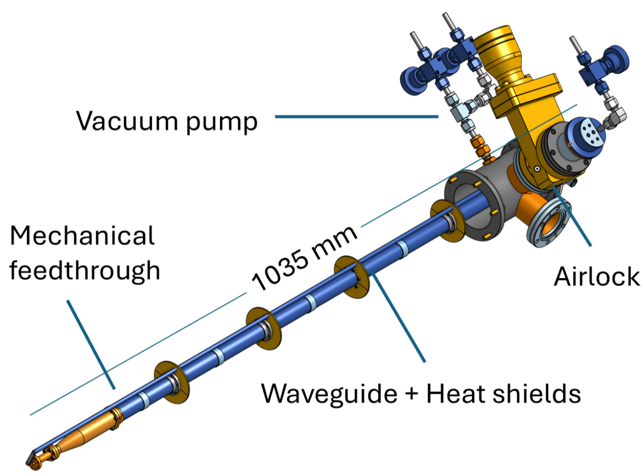

FIG. 5. The new high-field EPR probe is 1.035m long from end to end along the waveguide. This design features an airlock with a dedicated vacuum pump, and a mechanical feedthrough, providing the groundwork for the final designs presented here.

modified sample holder and transfer system adhere to.

1. Functional through large temperature gradient and at liquid helium temperatures (2 K - 300 K).

2. Functional through large pressure gradient, including low vacuum (20 mBar - 1 atm).

3. Made of non-magnetic materials : the probe lies at the center of a 16 T magnetic field.

4. Is completely self contained inside the magnet's 60mm bore.

5. Uses simple electronic devices, mostly a mechanical design. Common encoders and motion sensors lose sensitivity at high B values.

6. Reliably manufacturable on commerically available 3D printers.

7. Limits the amount of heat flowing into main chamber per cycle.

8. Limits the amount of vacuum lost per cycle, ideally leaving main vacuum untouched.

IV. PROPOSED DESIGN

The figures shown here were adapted from the two designs showcased earlier. Modifications were made using OnShape CAD software. Functionally, the new probe is identical to the current setup, microwaves are generated by some optical setup away from the magnet, and are directed towards the top of probe sitting in the magnet as shown in Fig. 6. From there, the waveguide sends microwaves down towards the sample. The main benefit of the system described here is the ability to house 9 samples at once, saving over 50 hours each cycle. Furthermore, the design allows easy access to the probe while installed, enabling high sample throughput.

A. Swivel

The sample holder has a few important modifications, which are shown in detail in Figure 7. Firstly is the swivel tray, which sits at the center of the modulation coil and houses two samples. A mechanical feedthrough provides a single degree of motion, rotation, which allows for the tray to move between two samples as shown in 7A. The coil holder has physical stops which keep the samples in the tray lined up with the waveguide and mirror assembly when flipped completely. In designing this part it was important to minimally modify the sample holder to avoid changing the optics inside the holder. By accommodating an extra sample, this part of the new design saves around 8 hours.

B. Sample Tabs

In this design, we chose to remove a point of uncertainty by designing sample "tabs", shown in Figure 8A. These "tabs" house the samples in a dedicated receptacle, which can then be moved in a predictable manner with the feedthroughs. The tabs utilize two 3D-printable parts which press a piece of mylar film between them to form a platform for the sample to sit on. Mylar is a good choice for this application, since it's extremely thin and essentially invisible at the high frequencies used in EPR experiments. Because of the

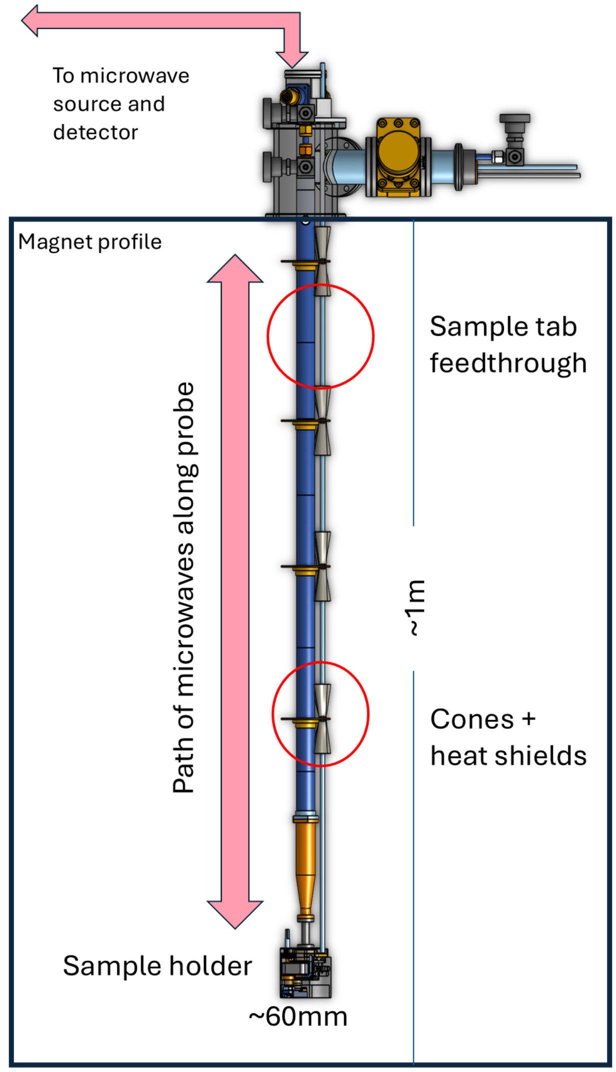

FIG. 6. Here is a rough cartoon showing what the probe looks like when placed in the magnet. Only the top section, with the airlock and vacuum pumps, shows. Microwaves travel a meter down towards the sample holder along the waveguide. This design has a feedthrough enabling sample movement through the heat shields with the help of cones. Every aspect of this design is discussed individually down below

high sensitivities achieved at high-field, sample volume can be kept low, and the sample tabs are small, less than 30mm in length and only 6mm across.

The sample tab also has space for a threaded insert, which will allow an external threaded rod to secure itself onto the sample. In Fig. 8B, we see there is a second mechanical feedthrough responsible for this action, which sits opposite of the first, towards the widest part of the swivel. This feedthrough offers two degrees of motion: translation and rotation, both along the main axis, allowing for deposition and collection of samples from the swivel. Beyond that, there is the ability for sample movement upwards, where it can be extracted

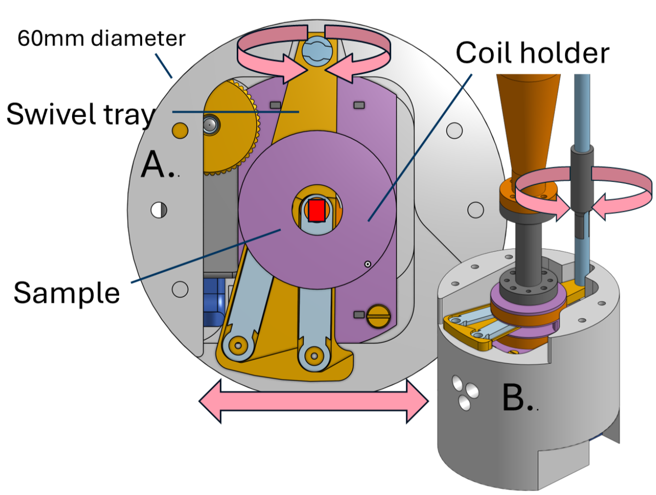

FIG. 7. (A) A top view of the modified sample holder. The swivel tray (yellow) is connected to a mechanical feedthrough which is able to rotate about it's center. This enables a swivel motion, where we can now switch between two samples.(B) An isometric view of how the sample holder and tray line up with the waveguide at the end of the probe (connecting flange not shown). Missing from this figure is the second feedthrough responsible for moving samples.

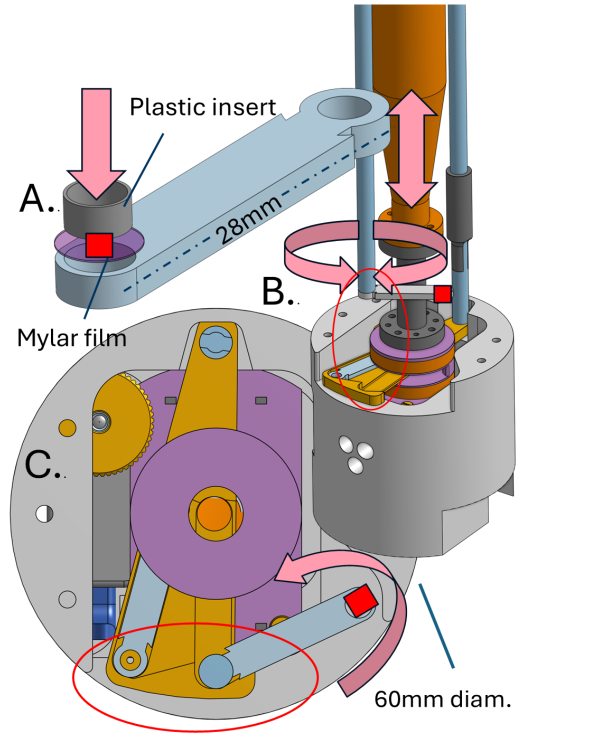

FIG. 8. (A) A piece of mylar film is pressed between a plastic insert and the main body to make the sample tab. These parts will be 3D printed, providing a robust way to house potentially delicate samples. (B) The mechanical feedthrough provides two degrees of motion. Circled, we see where the tab will dock in place with the swivel. Highlighted in red is the sample. (C) From a top view perspective, we see how the sample rotates into place once docked with a single motion.

from the probe altogether.

The geometry of the sample tray and modified sample holder allow enough room for the tabs to rotate smoothly into the desired positions as shown in Fig. 8C. Because the swivel is able to flip between both samples, it is possible to switch both samples out for new ones at any given time.

C. Moving Up

Once the sample tab is attached to the second mechanical feedthrough, it must go up towards the probe head in order to reach the airlock. Ideally this would be a trivial process, however Fig. 5 shows that there are a series of heat shields in the way, blocking a direct path towards the top.

The reason lies in the heat profile of the probe, shown in Fig. 9. At the bottom, samples reach temperatures as low as liquid helium (2 K) and the probe head is at room temperature, creating a roughly 300 K temperature gradient across the distance of a meter. In order to maintain this gradient, copper heat shields are installed to absorb incoming heat, cooling the surrounding air in the process. Since copper has a relatively high thermal conductance, it's great at holding onto heat, leading to a "compartmentalization" of temperature along the probe's main axis, where temperature increases step-wise between shields. These shields serve a second purpose, radiation isolation, meaning they block stray microwave sources from reaching the sample and causing unwanted excitations.

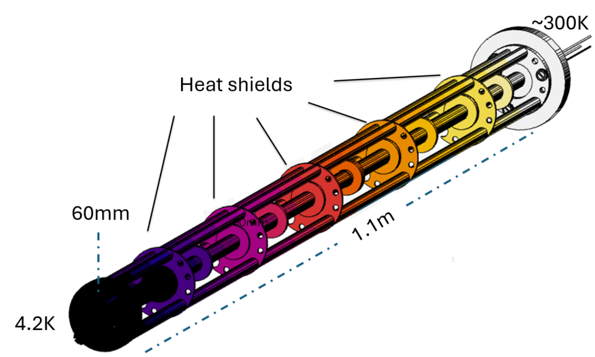

FIG. 9. Here, is the 300 K gradient across the 1.1m long EPR probe used in the ITST's 240 GHz setup. Image was produced using SimScale's Conjugate Heat Transfer (IBM) simulation.

It's clear that the copper shields are unavoidable from an experimental standpoint. In order to move the sample through them, we chose to create a cutout with millimetric tolerances. To reduce the flux of air flowing directly from the sample holder to the probe head, these cutouts were purposefully offset, creating a reduced cross-sectional area like the one shown in Figure 10A.

Though this addresses the thermal considerations, it makes it difficult to move the sample through consecutive shields since we do not know the precise angle and position of the sample tab relative to the cutout. This could potentially cause issues wherein a sample crashes into a shield, losing a sample and damaging the magnet.

The solution we came up with are what we call cones. Cones are about 80mm from end to end, and are designed to cover the entire range of motion of the sample tab in such a way that the tab is gradually aligned towards the shield cutouts as the cone tapers. Figures 10B and 10C show how this taper functions. The magnet and waveguide constrain the tab to the cone's opening, leaving no room for the sample tab to "escape." The cones themselves are designed to be 3D-printed, and are secured onto the copper heat shields with screws.

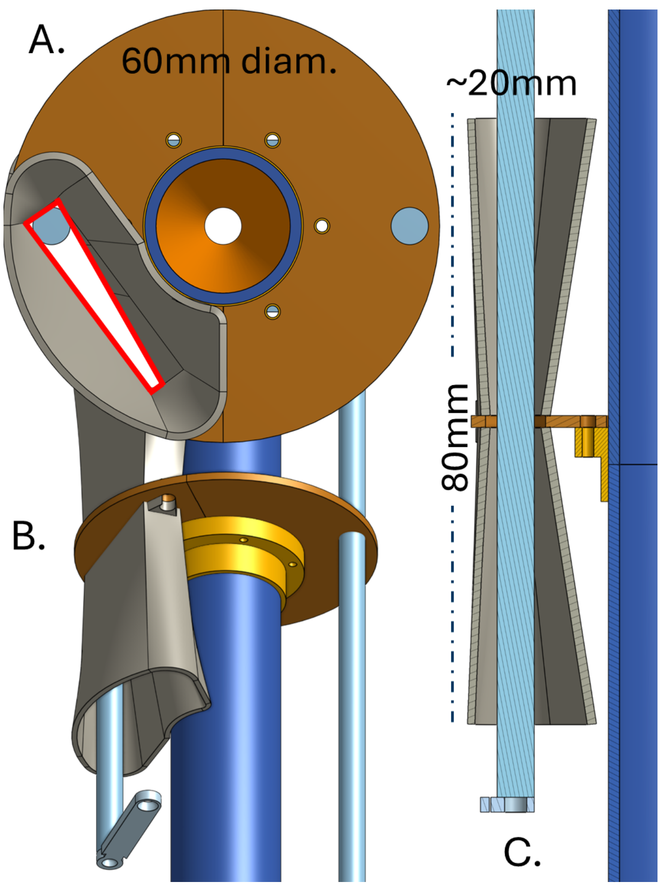

FIG. 10. (A) Offset cutouts reduce airflow along the probe. (B) The cone (gray) covers the entire range of motion of the sample. The waveguide (right) and magnet profile (not shown) keep the sample within this range. (C) The cones taper towards the cutouts gradually over a distance of 40mm on both ends because the design requires that the feedthrough cycles up and down along the probe to move samples.

D. Differential Pumping and Feedthroughs

It was discussed earlier how a strong vacuum (20 mbar) is necessary when it comes to collecting an EPR signal. It's important to understand how vacuum is maintained even as the feedthroughs cross from the exterior of the probe into the low pressure environment, without introducing outside air. It turns out that vacuum is maintained through a differential pumping system, shown in Figure 11. First, a main vacuum (vacuum A) is created inside of the magnet's main chamber. At the interface between the probe head and the mechanical feedthrough, lies an assembly of two Viton o-rings, intentionally separated by a teflon holder. Between these o-rings we create a second lower-pressure vacuum (vacuum B). The bottom o-ring, closest to vacuum A, ensures a proper seal between vacuum A and vacuum B. The top o-ring, closest to the outside, ensures a seal between vacuum B and the outside air. Since we create a controlled pressure gradient at the feedthrough-probe head interface, the o-rings are placed in ideal conditions, and both vacuums are maintained regardless of the motion of the feedthrough.

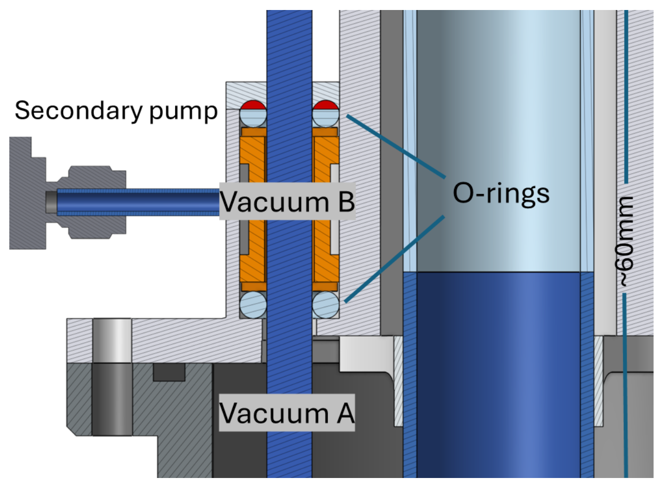

FIG. 11. Here is a cross-section of the feedthrough-o-ring interface. Shown in orange is the teflon o-ring holder. In light blue are the o-rings. In dark blue is the feedthrough that goes through the pressure gradient. We also see the vacuum pump responsible for vacuum B, and the point where vacuums A and B meet at the bottom o-ring. Not depicted here is the main vacuum pump, responsible for creating vacuum A which lies just below the assembly depicted here.

E. Airlock and Cartridge System

Once the sample is moved through each of the heat shields (4 in total), there needs to be a way to extract them from the inside of the magnet altogether. Part of that process entails being able to separate a small section of space from the main vacuum, enabling rapid access. We chose to achieve this by using a mechanical gate valve. As the "hand wheel" (Shown in yellow in Fig. 12B) is turned, a section of pipe protruding from the main probe body is closed off from the main chamber with a strong seal preventing vacuum leakage.

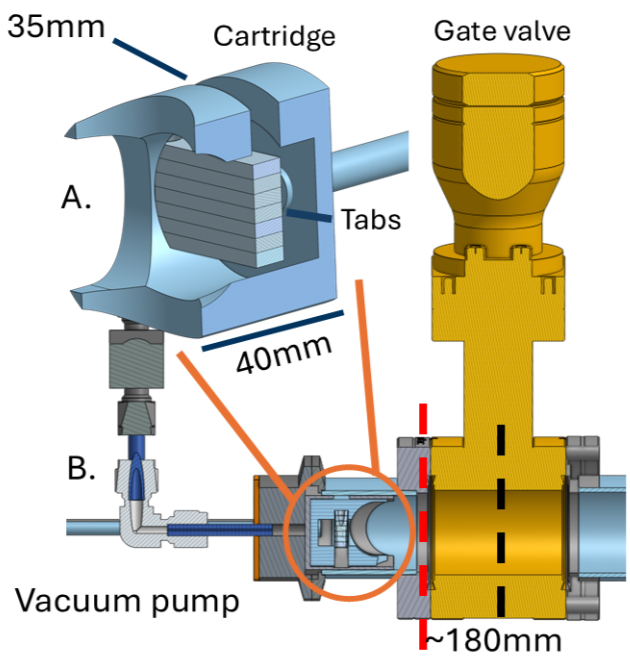

FIG. 12. (A) Here is an inside view of the cartridges (blue), with one chamber loaded completely with 7 sample tabs. (B) This is a cross-sectional view of the side pipe that has the gate valve (yellow) and cartridge system in place (circled in orange). The black dashed line shows where the gate valve will close the vacuum off, and the red dashed line shows where the connecting flange will be removed for access to the inside of the setup.

Samples will be accessed from the airlock using containers we call "cartridges." These cartridges, shown in Fig. 12A, are designed to hold 7 samples at once within a cross section of only 35mm in diameter, and have two separate chambers sitting perpendicular to each other; one for depositing old samples and the other for collecting new samples. Because the cartridges will be fully encapsulated inside of the side-pipe (Fig. 13), it was important to have a design that could guide itself toward the right position with simple movements. There are two guide curves which correspond to a distinct "chamber" in the cartridge. These guides are perpendicular and curved so they can press against the central waveguide and place the opening of a chamber inline with the mechanical feedthrough responsible for sample tab movement. There is an outer sleeve surrounding the cartridge, which has a single opening responsible for keeping samples tabs from falling out into the magnet when not docked properly.

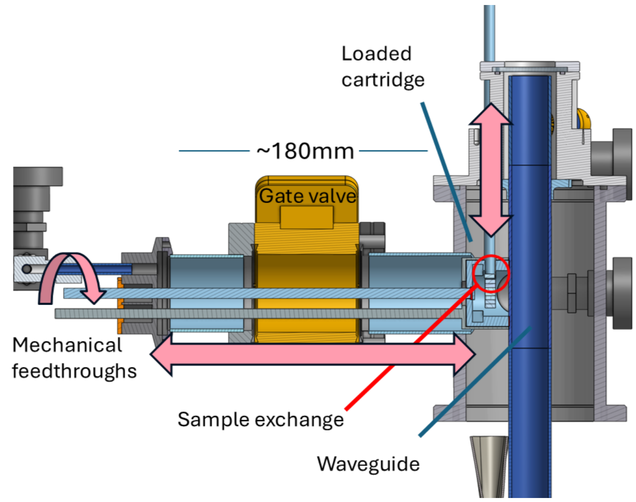

FIG. 13. Inside the side pipe, the cartridge feedthrough (blue) is able to rotate and move along its axis. Once docked, the sample tab feedthrough is raised or lowered to interact with samples in their respective chambers.

Inside of this side-pipe are two horizontal mechanical feedthroughs. The cartridge feedthrough (blue) is able to rotate and move along its axis. The sleeve feedthrough is only able to move along its axis. Figure 13 shows a still frame of the cartridge docked in place, and highlights all important degrees of freedom.

Once samples are in the cartridge, they can be pulled past the airlock, and a connecting flange can be removed, opening up a small section of pipe containing the entire cartridge assembly. After samples have been collected and replaced, this flange is reinstalled, and an dedicated pump creates a new vacuum in this reduced space. From the heat simulation shown earlier we don't expect this area to have cryogenic temperature but if ice formation becomes a problem, a dedicated heater can be placed around the load lock to prevent blockage.

V. EXPERIMENT

The new setup is not currently built, making it impossible to test the cones and cartridge system. We could, however, easily test the sample position inside of the swivel and identify possible issues with the design. A simplified version of the sample holder, Figure 14, was created and adapted to fit the ITST's 240 GHz EPR setup. Instead of the complex roof mirror assembly, which has been shown to work [7], we placed a simple flat mirror roughly 2.49mm (one wavelength) from the bottom sample. This creates standing wave conditions, placing the sample at a maximum of the magnetic field of incident radiation, minimizing signal losses.

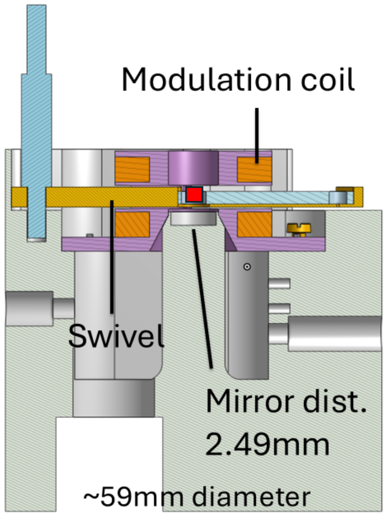

FIG. 14. This is a simplified version of the sample holder used for testing. Included is a modulation coil, and the swivel that sits inside of it. A flat mirror sits one wavelength below the sample (shown in red).

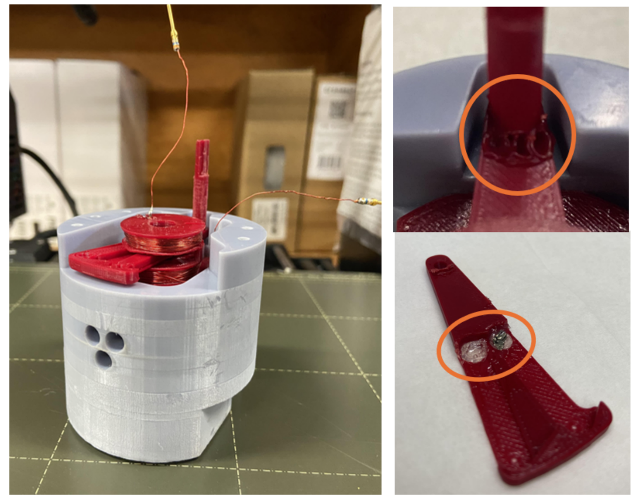

FIG. 15. Left: Fully assembled sample holder. The main body (gray) was printed out of resin on an Anycubic Photon Mono X 6Ks printer. The swivel and coil holder (red) were printed out of PLA on an Original Prusa 3D printer Top Right: Final welded swivel stick and sample tray. Welds were made by pressing a soldering iron at 200 C into the joint, fusing the two plastics. Bottom Right: Loaded sample tray with Tempol (left) and $NiPS_3$ (right) using high-vacuum grease.

A. Assembly

The main body was printed out of resin on an Anycubic Photon Mono X 6Ks resin printer using standard settings. After printing , the sample was placed in a bath of isopropyl alcohol for roughly 10 minutes and cured with UV light for about 30 minutes. The coil holder and sample tray were printed out of PLA with a solid infill pattern on an Original Prusa i3 MK3 3D printer. A modulation coil was wound using 30 gauge enameled copper mag-wire. Each section of the coil had approximately 200 turns and was set with a clear varnish. Brass leads were soldered to the wire ends. The complete prototype is shown in Figure 15.

The samples we used were crystalline $NiPS_3$ and a polystyrene-encased Tempol; here, Tempol is a common EPR reference sample and can be used to normalize unknown signals. These samples were larger than what the sample tabs were designed for, so instead we used high-vacuum grease to keep the samples in place, as shown in Figure 15. One samples were situated in the swivel, they were placed inside of the modulation coil and a plastic rod (the "swivel-stick") was melted to it using a soldering iron at approximately 290 C, ensuring a good connection. The "welds" described here are also shown in Figure 15.

B. Methods and Measurement

The samples were cooled to around 100 K using liquid nitrogen over the period of roughly an hour. Measurements were taken at a main field of approximately 8.65T. Samples were irradiated with 240 GHz microwaves at 40 mwatts. Amplitude was plotted as the magnetic field was modulated around the main field. For Tempol at room temperature, a significant number of splitting phenomenon are not detectable, leading to a single peak in the spectra at around -10 mT. The noticeable increase in detail at low temperatures shows that the sample holder maintains the sample in the proper position, even at cryogenic temperatures. Overall, the 300K and 100K Tempol/PS signals seem to match up with the literature [8], given some modulation. Here, Tempol is encased in solid polystyrene so this sample's signal at 100 K, shown in Figure 16, contains contributions from all anisotropic states leading to unique peaks at -30 mT, -10 mT, and 10 mT respectively.

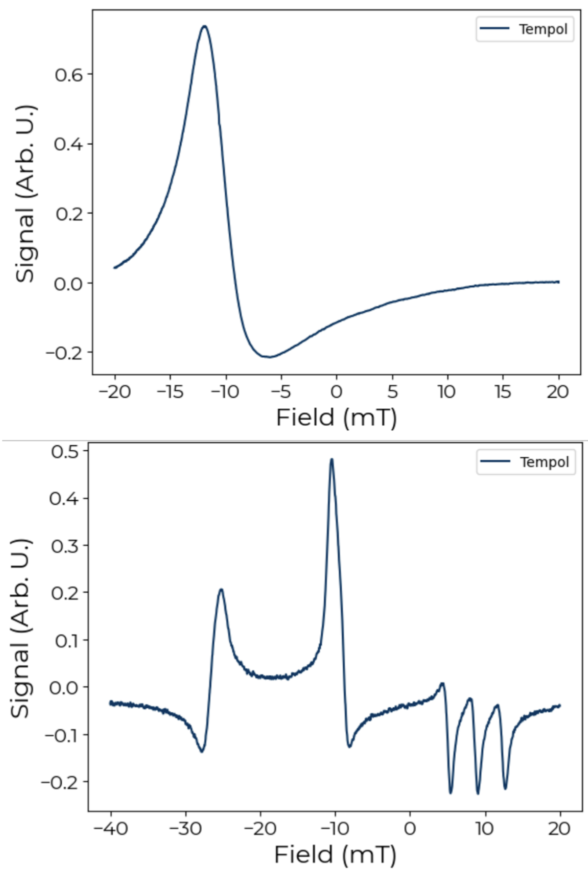

FIG. 16. Main field approx. 8.65T. Samples irradiated with 240 GHz microwaves at 40 mwatts.Amplitude was plotted as the magnetic field was modulated. Top: Tempol reference at room temperature. Bottom: The same tempol Reference at 100 K.

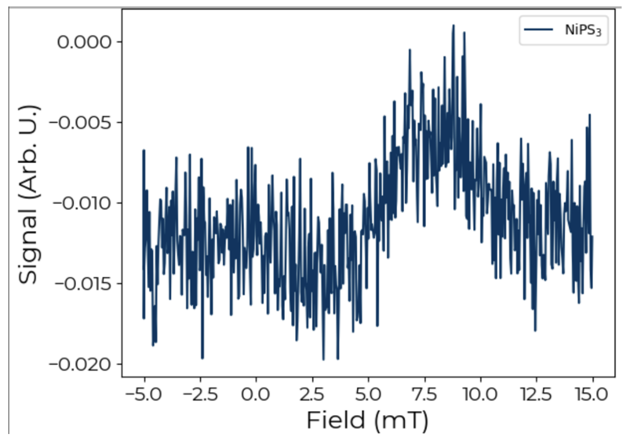

FIG. 17. Main field approx. 8.65T. Samples irradiated with 240 GHz microwaves at 40 mwatts.Amplitude was plotted as the magnetic field was modulated. Shown here is the room temperature spectra of $NiPS_3$

At room temperature we were able to swivel, and collect a spectra for the $NiPS_3$ sample. Unfortunately, some tolerances changed as temperatures cooled, and at 100 K we ended up snapping a coupling that connected to the swivel-stick when we tried moving the feedthrough. There is no 100K measurement for the $NiPS_3$ sample. The initial signal, seen in Figure 17, is extremely noisy, but has a single peak at approx. 8 mT, which matches the shape of signals seen in other experiments [9].

VI. CONCLUSION AND FUTURE WORK

Though the proof of concept was not entirely successful, there was strong evidence from the room temperature comparisons that continued testing and design modifications will lead to a more robust product. Further experimentation with low-temperature filaments, or machined parts offers opportunities for improvement. Once the new EPR setup is built, more rigorous testing will ensue on the other feedthroughs, the cones, and cartridge system discussed earlier. Beyond that, once the mechanical system is optimized, it leads to the possibility for complete automation of sample transfers via simple motors and smart sensor choices, reducing the time needed to collect spectra for large sample volumes by as much as 50 hours per cycle.

On a broader scale, it's important to note that the sample holder used here was built and tested in the time span of a few weeks. The engineering process from an idea to a physical piece of instrumentation lends itself well to experimental settings. 3D printing technology is getting better everyday, and offers the possibility for extremely accessible, custom built lab equipment. Ultimately this project serves as one of the many up and coming cases for CAD and non-conventional manufacturing methods in physics.

ACKNOWLEDGMENTS

I would like to acknowledge Dr. Mark Sherwin, Dr. Antonín Sojka, and the rest of the Sherwin Group (especially Brad, Alex, and Johanna) for their continued guidance and support. I thank Dr. Sathya Guruswamy for inviting me to participate in the program, and the NSF for supporting this research with REU grant PHY-2349677.

[1] F. H. C. U. G. S. T. Z. Peng, T. Biktagirov, "Investigation of near-surface defects of nanodiamonds by high-frequency epr and dft calculation," *J. Chem. Phys* (2019) .

[2] S. Maity, B. D. Price, C. B. Wilson, A. Mukherjee, M. Starck, D. Parker, M. Z. Wilson, J. E. Lovett, S. Han, and M. S. Sherwin, "Triggered functional dynamics of aslov2 by time-resolved electron paramagnetic resonance at high magnetic fields," *Angewandte Chemie International Edition* **62** no. 13, (2023) e202212832.

[3] Nakarada, U. Glavinić, M. Ristanić, M. Popović, J. Stevanović, Z. Stanimirović, and M. Mojović, "Bridging the buzz: In vivo epr imaging unlocking the secrets of honey bee health," *Journal of Experimental Zoology Part A: Ecological and Integrative Physiology* (2024) .

[4] H. M. S. et al., "Advances in probes and methods for clinical epr oximetry," *Advances in Experimental Medicine in Biology* (2014) .

[5] K. Möbius and A. Savitsky, "High-field/high-frequency epr spectroscopy in protein research: Principles and examples," *Applied Magnetic Resonance* (2023) 207–287.

[6] A. Sojka, M. Šedivỳ, A. Lagiň, A. Gabriš, T. Láznička, V. T. Santana, O. Laguta, and P. Neugebauer, "Sample holders for sub-thz electron spin resonance spectroscopy," *IEEE Transactions on Instrumentation and Measurement* **71** (2022) 1–12.

[7] A. Sojka, B. D. Price, and M. S. Sherwin, "Order-of-magnitude snr improvement for high-field epr spectrometers via 3d printed quasi-optical sample holders," *Science Advances* **9** no. 38, (2023) eadi7412.

[8] Y. S. M. N. I. N. K. F. K.-I. M. Yusuke Makino, Megumi Ueno, "Simplifying quantitative measurement of free radical species using an x-band epr spectrometer," *J Clin Biochem Nutr.* (2022) .

[9] F. Wang, N. Mathur, A. N. Janes, H. Sheng, P. He, X. Zheng, P. Yu, A. J. DeRuiter, J. R. Schmidt, J. He, and S. Jin, "Defect-mediated ferromagnetism in correlated two-dimensional transition metal phosphorus trisulfides," *Science Advances* **7** no. 43, (2021) eabj4086.